LETTER

Correlation corrected phonon vibration in $YTiO_3$ and its effect on electronic properties

To cite this article: Xiaoping Yang and Gang Wu 2017 *EPL* **117** 27004

A Letters Journal Exploring the Frontiers of Physics

January 2017

EPL, **117** (2017) 27004
doi: 10.1209/0295-5075/117/27004

www.epljournal.org

Correlation corrected phonon vibration in $YTiO_3$ and its effect on electronic properties

Xiaoping Yang[1(a)] and Gang Wu[2(b)]

[1] *High Magnetic Field Laboratory of the Chinese Academy of Sciences - Hefei 230031, PRC*
[2] *Institute of High Performance Computing - 1 Fusionopolis Way, L16-16 Connexis, Singapore 138632, Singapore*

received 3 November 2016; accepted in final form 16 February 2017
published online 7 March 2017

PACS 72.80.Ga – Transition-metal compounds
PACS 78.30.-j – Infrared and Raman spectra
PACS 71.27.+a – Strongly correlated electron systems; heavy fermions

Abstract – The infrared (IR) phonon vibration of the narrow t_{2g} band system $YTiO_3$ and its effect on electronic properties are studied using the generalized gradient approximation (GGA) and its combination with Coulomb correlation U. Coulomb U is found to improve the GGA results not only in electronic properties which has been researched frequently, but also in its lattice dynamics. The phonon frequency is increased effectively, especially in high-frequency region, which corrects the gap between experimental and theoretical GGA result. More importantly, IR-active modes are found to affect electronic properties significantly, and we find vibration-sensitive magnetic exchange interaction and strong electron-phonon coupling.

Introduction. – The t_{2g} band perovskite $R\mathrm{TiO_3}$ (R is a rare-earth cation) owns rich spin/orbital ordered phases, due to the couplings among charge, orbital, lattice, and spin degrees of freedom. These emergent phases hold promising potential for novel tailor-made functionalities useful in, *e.g.*, microelectronics, spintronics, and correlated-electron devices. $YTiO_3$ with configuration $3d^1(t_{2g}^1)$ is a prototypical Mott-Hubbard insulator with ferromagnetic (FM) ground state below $T_C \sim 30\,\mathrm{K}$, and the t_{2g} orbitals have much stronger localized character due to the weak p-d hybridization. Static G-type orbital ordering was predicted theoretically [1,2] and confirmed in nuclear magnetic resonance [3] and several other experiments [4–12]. And its mechanism was investigated in detail by theoretical studies [13–17]. In contrast to these experimental and theoretical findings, the observation of an isotropic, small-gap spin-wave spectrum both in FM $YTiO_3$ and also in antiferromagnetic (AFM) $LaTiO_3$ was taken as evidence for strong orbital fluctuations [18,19], which was supported also by NMR [20] and Raman studies [21]. An alternative explanation of orbital liquid, compatible with orbital order, was proposed [16]. However, the predicted contribution to the specific heat from the orbital liquid has not been observed in $LaTiO_3$ [9].

Although the above intensified research was done, the physical properties of $YTiO_3$ are far from being fully understood. Motivated by a recent experimental study of Li *et al.* [22], which indicates that strong localized atomic fluctuations may be linked to a fluctuating $GdFeO_3$-type distortion that correlates to tilting angle, and finally affect the electronic properties of $YTiO_3$, we carry out a theoretical investigation on lattice dynamics and its influence on the electronic properties. Coulomb correlation U is found to improve the generalized gradient approximation (GGA) and the spin-polarized generalized gradient approximation (SGGA) results not only in the electronic property that has been researched frequently, but also in lattice dynamics. Good agreement is observed between experimental and theoretical infrared (IR) frequencies. Furthermore, deformation potential calculations reveal vibration-sensitive magnetic exchange interaction and strong electron-phonon coupling in $YTiO_3$.

Methods. – We carry out the numerical calculations using the Vienna *ab initio* Simulation Package (VASP) [23] within the GGA framework (Perdew-Burke-Ernzerhof exchange correlation functional) [24]. The ion-electron interaction is modelled by the projector augmented-wave

(a) E-mail: xpyang@hmfl.ac.cn
(b) E-mail: wug@ihpc.a-star.edu.sg

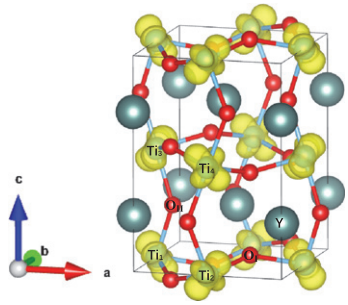

Fig. 1: (Color online) Crystal structure and G-type orbital ordering of orthorhombic $YTiO_3$ with space group *Pbnm*.

(PAW) method [25] with a uniform energy cutoff of 500 eV. In order to treat the effect of local Coulomb interactions in a partially filled $3d$ band of Ti, the GGA$+U$ method is applied [26]. The Brillouin zone (BZ) is sampled with the $9\times9\times7$ mesh with its origin at the Γ-point. The valence states include $2s$, $2p$ for O, $4s$, $4p$, $4d$, $5s$ for Y, $3p$, $3d$, $4s$ for Ti atoms.

$YTiO_3$ has an orthorhombic crystal structure (space group *Pbnm*, D_{2h}^{16}) with 4 f.u./unit cell (see fig. 1), which incudes 4 Ti sites (sites 1 and 2 in one layer, with sites 3 and 4 on top of 1 and 2, respectively). The lattice constants are set to experimental values: $a = 5.316$ Å, $b = 5.679$ Å, and $c = 7.611$ Å [27]. GGA and SGGA electronic structure calculations give nonmagnetic metallic and FM half-metallic ground state, respectively [1]. Both of them fail in the prediction of the insulating ground state of $YTiO_3$. The reason is an underestimation of the strong correlations in the density functional theory. The internal atomic coordinates are relaxed in lattice dynamics research. In our GGA + U calculation, the parameters $U = 4.5$ eV, $J = 0.62$ eV are used to reproduce the FM ground state and experimental band gap [28] (about 1.2 eV) properly. The obtained magnetic moment of 0.83 μ_B per Ti atom is also in excellent agreement with experimental value of 0.85 μ_B [4].

The phonon vibrational frequency at the Γ-point is investigated in detail by using the frozen-phonon method which constructs the force-constant matrix by a small-displacement method in the harmonic approximation [29,30]. Then we can obtain the dynamical matrix by a Fourier transformation. The phonon frequencies and vibrational modes can be obtained by diagonalizing the dynamical matrix directly. The internal atomic coordinates are fully optimized before performing force constants calculation. Finally, the optimal structure is obtained when the residue forces acting on all the atoms were less than 0.001 eV/Å.

The infrared intensity of the ν-th vibrational mode is defined as

$$f(\nu) \propto \sum_{\alpha} \left|(\bar{Z}^*_{\nu})_{\alpha}\right|^2 = \sum_{\alpha} \left| \sum_{s\beta} Z^*_{\alpha\beta}(s)(m_0/m_s)^{\frac{1}{2}} e_{\beta}(s|\nu) \right|^2, \quad (1)$$

where Z^*(s) is the Born effective charge tensor for atom s, m_s its mass, $e_\beta(s|\nu)$ the component of the normalized dynamical matrix eigenvector for mode ν involving atom s in the Cartesian direction β, $(\bar{Z}^*_{\nu})_{\alpha}$ the mode effective charge in the α-direction for a given mode ν, and m_0 an arbitrary mass. We choose m_0 =1 in this work. Finally, the components of the Born effective charge tensor for a given atom s are expressed as follows:

$$Z^*_{\alpha\beta}(s) = V\frac{\partial P_\alpha}{\partial r_\beta(s)}, \quad (2)$$

where r_β is the atomic coordinate in the β-direction, V the volume per unit cell, and P_α the polarization tensor which can be obtained by using the King-Smith and Vanderbilt (KSV) method [31]. So the physical meaning of $Z^*_{\alpha\beta}(s)$ is the induced polarization of the solid along the α-direction by a unit displacement in the β-direction of the atomic sublattice.

Results and discussion. –

Phonon. For $YTiO_3$, a factor-group analysis yields a total number of 60 Γ-point phonons, of which 24 ($7A_g + 7B_{1g} + 5B_{2g} + 5B_{3g}$) are Raman-active modes, 25 ($7B_{1u} + 9B_{2u} + 9B_{3u}$) are infrared-active modes, 8 (A_u) are silent modes, and 3 ($B_{1u} + B_{2u} + B_{3u}$) are acoustic modes. The IR phonon frequencies obtained by different calculation methods are shown in table 1.

At first sight, GGA and SGGA results seem to give a similar frequency value. But the detailed analysis on the eigenvectors reveals that the order of vibrational modes with the increasing frequency is different, mainly in the low-frequency area below 410 cm^{-1} for B_{2u} and B_{3u}. This difference indicates the possible role of spin-phonon coupling in $YTiO_3$. Comparing the SGGA result with the GGA + U one, we find a good agreement in the order of vibrational modes. The effect of Coulomb U is embodied in increasing the phonon frequency, especially in the high-frequency region. To a large extent, Coulomb U really corrects the gap between experimental and theoretical-SGGA results, as we expected. On the whole, our GGA + U results are reasonable, the full set of IR phonon modes is generated and the obtained phonon frequencies agree well with the experimental values.

The Born effective charge tensors in GGA-, SGGA- and GGA + U-optimized structures are shown in table 2. The nominal ionic charges of Y, Ti, and O are 3, 3, and −2, respectively. Like other ABO_3 perovskites, the Born effective charge are generally larger than the corresponding nominal charges, especially for Y. When ferroelectric relaxation occurs, it has been found that the accompanying polar distortions make effective charges become closer to their nominal values. Here, it is noteworthy to mention that relatively large off-diagonal components appear in the Born effective charge tensors of $YTiO_3$ due to nonpolar distortion of the TiO_6 octahedron, which breaks the cubic symmetry in ABO_3 perovskites. GGA results deviate considerably from the nominal charges of

Table 1: IR-actived normal modes frequencies (in cm^{-1}) with irreducible representation B_{1u}, B_{2u} and B_{3u} of point group D_{2h} obtained by GGA, SGGA and GGA + U methods.

IR	GGA	SGGA	GGA + U	(Exp. [32,33])
	145.3	168.4	177.4	165
	187.3	187.4	211.8	203
	292.3	300.1	324.4	322
B_{1u}	329.0	326.7	355.2	349
	361.0	353.1	408.4	386
	484.7	494.1	564.3	543
	551.2	523.3	577.3	563
	125.1	129.5	146.2	139
	163.9	226.8	243.1	240
	227.6	237.7	278.2	273
	262.2	292.7	324.5	309
B_{2u}	322.2	344.7	369.2	364
	363.9	354.8	397.1	380
	406.0	436.0	491.3	462
	492.5	484.2	545.8	529
	511.5	512.0	571.5	578
	131.8	133.2	151.7	154
	191.1	193.8	218.5	210
	287.6	301.2	328.9	316
	305.0	315.9	341.9	336
B_{3u}	316.2	318.3	364.0	347
	382.3	390.4	434.3	428
	397.5	394.9	449.7	516
	483.3	486.7	527.3	554
	537.1	531.2	594.8	577

Table 2: Born effective charge tensors (in $|e|$) for structure optimized by GGA, SGGA and GGA + U. The axis x, y and z are defined as the [100], [010] and [001] directions of the unit cell.

Z^* (GGA)	Y	Ti	O_I	O_{II}
xx	4.6749	3.1820	−2.6855	−2.2146
xy	1.7711	−1.8709	−0.5032	−0.2904
xz	−0.3108	1.7111	0.7352	0.0411
yx	1.2242	−4.0145	−0.9807	3.3418
yy	6.4326	5.8415	−4.1462	−3.8818
yz	−0.1220	1.3731	−0.7750	0.0239
zx	0.0	2.2637	0.0981	0.0
zy	0.0	−1.6526	1.3703	0.0
zz	5.2841	4.2193	−2.5823	−4.0343
Z^* (SGGA)	Y	Ti	O_I	O_{II}
xx	3.9460	2.9185	−2.1919	−1.5358
xy	−0.4691	−0.9204	−0.8688	−0.6210
xz	−0.0682	−0.8195	−0.8288	0.5339
yx	−0.0492	−2.3950	0.0393	0.4251
yy	4.2080	6.2422	−3.7713	−2.6596
yz	0.0296	1.8546	−1.3629	−0.1703
zx	0.0	1.3514	0.5075	0.0
zy	0.0	−0.3926	0.2474	0.0
zz	4.0193	3.1872	−1.6864	−3.8852
Z^* (GGA + U)	Y	Ti	O_I	O_{II}
xx	4.1332	3.5220	−2.5717	−2.5959
xy	0.2876	0.2488	−0.5272	−0.5151
xz	−0.0315	0.1004	0.0857	0.05505
yx	0.2191	0.4661	−0.4654	−0.643
yy	4.0546	3.4705	−2.7052	−2.0074
yz	−0.009	−0.2077	−0.1573	−0.0243
zx	0.0	0.3081	0.1112	0.0
zy	0.0	−0.2768	−0.1648	0.0
zz	3.7978	3.6003	−2.0804	−3.2498

Y, Ti and O, not only in diagonal terms but also in off-diagonal terms. When the spin degree of freedom is taken into account in SGGA, the deviation is weakened greatly, but Z^*_{yy} of the Ti atom reaches an unreasonable value of 6.2422. Finally, the introduction of correlation U on Ti-d orbitals corrects Z^*_{yy} to a more reasonable value of 3.4705. As shown in eq. (1), the values of Born effective charges determine the infrared intensity. However, it is less meaningful to discuss the peak strength in GGA- and SGGA-IR spectra, giving that their peak positions already present a big error.

In $YTiO_3$, the oscillator strength vectors for the three IR-active modes B_{1u}, B_{2u} and B_{3u} are along the c, b and a axes, respectively. In order to compare with experimental data, we show IR spectra in fig. 2. For B_{1u} and B_{2u} modes, good agreement is obtained in the evolution of IR intensity between theory and experiment, only except for the highest one or two frequencies (564.3 and 577.3 cm^{-1} for B_{1u}, 571.5 cm^{-1} for B_{2u}). For the B_{1u} mode at 564.3 cm^{-1}, atomic displacements almost only occur within the ab plane, and so its oscillator intensity along the c-axis is weak and cannot clearly be seen in fig. 2. For B_{3u} modes below 410 cm^{-1}, the theoretical result gives a change trend similar to the experimental one. It should be noted that the intensity of the respective highest frequency of the B_{1u}, B_{2u} and B_{3u} modes is weakest and almost disappears in the experimental IR-active spectrum. Whether this is due to finite-temperature effects or LO-TO splitting remains to be seen.

Perturbation of phonon vibration on electronic properties. Finally, we discuss the change of self-consistent GGA + U energy bands, *i.e.*, the deformation potentials, and the nearest-neighboring magnetic exchange coupling constants J_{ab} and J_c by moving the atoms according to the eigenvectors $(e(s|\nu)/\sqrt{m_s})$ of IR-active modes at the Γ-point. Please see the supplementary material `Supplementarymaterial.pdf` for specific atomic displacement patterns of every IR-active phonon modes. Deformation potential calculation results are shown in figs. 3–5, where spin-up band structures for the

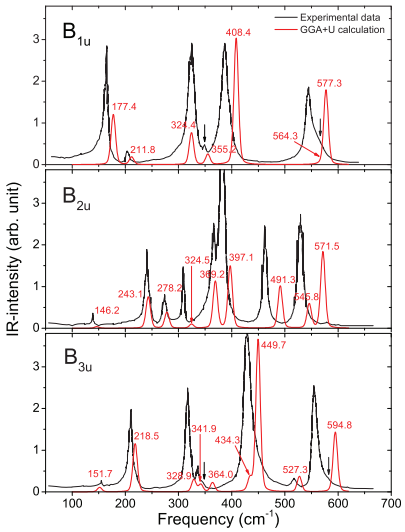

Fig. 2: (Color online) IR-active spectrum $f(\nu)$ obtained by GGA $+\,U$. The smearing width is $10\,\mathrm{cm}^{-1}$. The experimental data is from fig. 5 of ref. [32].

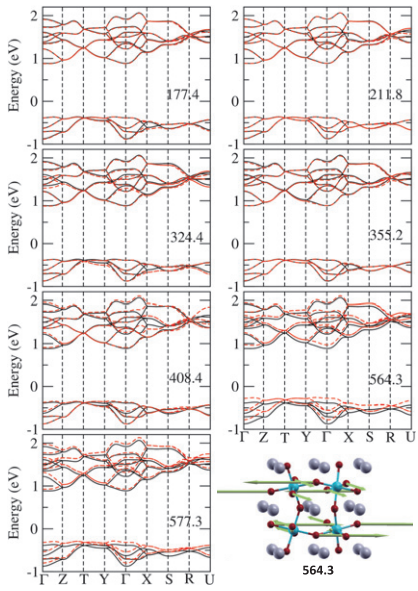

Fig. 3: (Color online) The change of self-consistent spin-up Ti-t_{2g} energy bands from atomic displacements of the B_{1u} phonon eigenvectors obtained by GGA $+\,U$. Full black (dashed red) lines are for the absence (presence) of atomic displacements. The Fermi level without displacements is set at zero. The inset is the atomic displacement patterns for B_{1u} at $564.3\,\mathrm{cm}^{-1}$.

undistorted (black line), and the distorted (dashed red line) lattices are plotted in the vicinity of the Fermi level to illustrate the crucial change in the electronic structure. High-symmetry K-points are at $\Gamma(0\ 0\ 0)$, $Z(0\ 0\ 0.5)$, $T(0\ 0.5\ 0.5)$, $Y(0\ 0.5\ 0)$, $X(0.5\ 0\ 0)$, $S(0.5\ 0.5\ 0)$, $R(0.5\ 0.5\ 0.5)$ and $U(0.5\ 0\ 0.5)$. The energy value in longitudinal coordinates is obtained by subtracting the Fermi energy of the system without distortion from the absolute energy of the system with or without distortion. We do not show

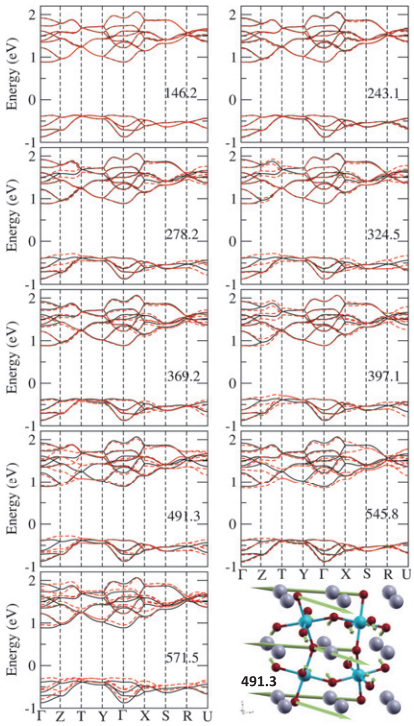

Fig. 4: (Color online) The change of self-consistent spin-up Ti-t_{2g} energy bands from atomic displacements of the B_{2u} phonon eigenvectors obtained by GGA $+\,U$. Full black (dashed red) lines are for the absence (presence) of atomic displacements. The Fermi level without displacements is set at zero. The inset is the atomic displacement patterns for B_{2u} at $491.3\,\mathrm{cm}^{-1}$.

the spin-down band structures, because a very large insulating gap covers the energy region of -3.0–$1.0\,\mathrm{eV}$, as discussed in the study of Sawada *et al.* [1].

Compared to the B_{2u} and B_{3u} modes, atomic motion from the B_{1u} modes has less influence on band structures. The atomic displacements of three IR modes mainly locate at Ti, O_I and O_{II} atoms. The larger Y atomic motion emerges only in first two low-frequency modes of B_{2u} and B_{3u}, but does not induce a big change of the energy bands. In addition, we find that the high-frequency modes of B_{1u}, B_{2u} and B_{3u} are always contributed mainly from the oxygen atomic motion, some of which lead to considerable bands evolution, *e.g.*, B_{2u} mode at $491.3\,\mathrm{cm}^{-1}$ and B_{3u} mode at $434.3\,\mathrm{cm}^{-1}$. Generally, atomic displacements from phonon eigenvectors really modify the energy bands, and even in some of the B_{2u} and B_{3u} modes lift greatly the degenerate of Ti-t_{2g} energy bands or energy points. Energy splitting in valence bands can reach a maximum value of 0.3 eV in the B_{2u} mode at $491.3\,\mathrm{cm}^{-1}$, indicating the strong electron-phonon coupling in $YTiO_3$.

Introducing of atomic displacement does not alter the ascending order of magnetic states in total energy FM→A-AFM→C-AFM→G-AFM, and the FM state always remains the ground state of the system. However, the deformation potential caused by atomic motion leads

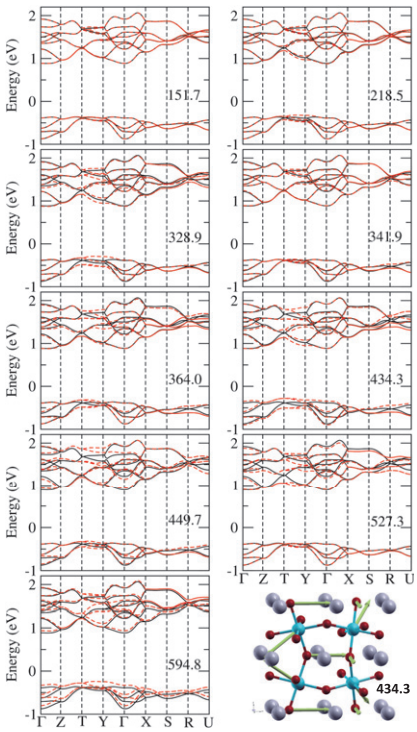

Fig. 5: (Color online) The change of self-consistent spin-up Ti-t_{2g} energy bands from atomic displacements of the B_{3u} phonon eigenvectors obtained by GGA + U. Full black (dashed red) lines are for the absence (presence) of atomic displacements. The Fermi level without displacements is set at zero. The inset is the atomic displacement patterns for B_{3u} at 434.3 cm^{-1}.

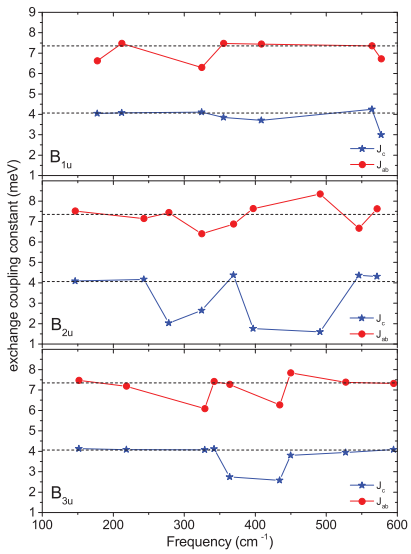

Fig. 6: (Color online) Magnetic exchange coupling constants, in-plane J_{ab} and out-of-plane J_c, obtained by deformation potential calculations. Horizontal dashed lines label the exchange coupling constants without atomic displacements.

to the change of the magnetic exchange coupling constant J, and the detailed results are given in fig. 6. In agreement with the above discussion on the band structure, the atomic motion from the B_{1u} modes induces the weakest change of the $J_{ab}(J_c)$ value. And the B_{2u} modes are found to affect greatly the $J_{ab}(J_c)$ value, *e.g.*, the change from the original 7.35(4.06) meV to 8.34(1.59) meV after introducing O_{II}-dominated atomic displacements from the B_{2u} phonon eigenvector at 491.3 cm^{-1}. Generally, the presence of strong electron-phonon coupling leads to a reduction of the J value, due to the renormalization by polaronic effects [34]. At the same time however, the effective on-site Coulomb repulsion is reduced due to the attractive interaction which eventually leads to on-site bipolaron formation at sufficiently strong coupling [34,35]. This would tend to enhance the magnetic exchange coupling J. Therefore, one would expect two different effects going in the opposite directions, just like the changes of in-plane J_{ab} and out-of-plane J_c, respectively, for B_{2u} at high frequency 491.3 cm^{-1}. A more detailed analysis of the evolution of J_{ab} and J_c with the change of electron-phonon coupling strength is worthy of being carried out to further understand the underlying mechanism of the observed trend in the change of magnetic exchange coupling.

In a word, phonon vibration has a significant influence on the electronic properties of $YTiO_3$, especially the B_{2u} and B_{3u} modes, which could be the underlying reason of some anomalous physical phenomena, *e.g.*, the nearly isotropic experimental spin-wave spectrum reported by Ulrich *et al.* [18]. We hope that our theoretical findings can bring to a more detailed study on spin-phonon and orbital-phonon couplings in the future, in order to understand deep-seated physics in $YTiO_3$ and even other t_{2g} systems.

Summary. – We have investigated lattice dynamics of the narrow t_{2g} band system $YTiO_3$ using the first-principles method, and made comparisons with experimental results. The complete set of zone center IR phonon modes and their spectra intensity are calculated by using the frozen-phonon method and the modern theory of the polarization method. The incorporation of the Coulomb correlation U is found to improve the GGA and SGGA results not only in the electronic property that has been researched frequently, but also in its lattice dynamics. Good agreement is observed with experimental frequencies. The effect of phonon vibration on the electronic properties is discussed in the detail by the change of self-consistent energy bands and magnetic exchange coupling constants. IR-active modes affect the electronic properties significantly, and we find vibration-sensitive magnetic exchange interaction and strong electron-phonon coupling. Finally, we note that phonon anomaly and photoemission kink discovered experimentally may result from an increase in electron-phonon coupling due to enhanced electronic correlations or reduced screening not included in the density functional theory [36–38]. In our study, we already introduced the correlation U in phonon vibration calculations, however this potential issue may not be solved totally.

* * *

This work was supported by the National Natural Science Foundation of China under Grant Nos. 11644001, 11674325 and U1632162, and the A*STAR Computational Resource Centre of Singapore through the use of its high-performance computing facilities.

REFERENCES

[1] Sawada H. and Terakura K., *Phys. Rev. B*, **58** (1998) 6831.
[2] Mizokawa T. and Fujimori A., *Phys. Rev. B*, **54** (1996) 5368.
[3] Itoh M., Tsuchiya M., Tanaka H. and Motoya K., *J. Phys. Soc. Jpn.*, **68** (1999) 2783.
[4] Akimitsu J., Ichikawa H., Eguchi N., Miyano T., Nishi M. and Kakurai K., *J. Phys. Soc. Jpn.*, **70** (2001) 3475.
[5] Nakao H., Wakabayashi Y., Kiyama T., Murakami Y., Zimmermann M., Hill J. P., Gibbs D., Ishihara S., Taguchi Y. and Tokura Y., *Phys. Rev. B*, **66** (2002) 184419.
[6] Iga F., Tsubota M., Sawada M., Huang H. B., Kura S., Takemura M., Yaji K., Nagira M., Kimura A., Jo T., Takabatake T., Namatame H. and Taniguchi M., *Phys. Rev. Lett.*, **93** (2004) 257207.
[7] Tsubota M., Igay F., Uchihira K., Nakano T., Kura S., Takabatake T., Kodama S., Nakao H. and Murakami Y., *J. Phys. Soc. Jpn.*, **74** (2005) 3259.
[8] Kubota M., Nakao H., Murakami Y., Taguchi Y., Iwama M. and Tokura Y., *Phys. Rev. B*, **70** (2004) 245125.
[9] Fritsch V., Hemberger J., Eremin M. V., Krug von Nidda H.-A., Lichtenberg F., Wehn R. and Loidl A., *Phys. Rev. B*, **65** (2002) 212405.
[10] Cwik M., Lorenz T., Baier J., Müller R., André G., Bourée F., Lichtenberg F., Freimuth A., Schmitz R., Müller-Hartmann E. and Braden M., *Phys. Rev. B*, **68** (2003) 060401.
[11] Hemberger J., Krug von Nidda H.-A., Fritsch V., Deisenhofer J., Lobina S., Rudolf T., Lunkenheimer P., Lichtenberg F., Loidl A., Bruns D. and Büchner B., *Phys. Rev. Lett.*, **91** (2003) 066403.
[12] Eitel M. and Greedan J. E., *J. Less-Common Met.*, **116** (1986) 95.
[13] Mizokawa T., Khomskii D. I. and Sawatzky G. A., *Phys. Rev. B*, **60** (1999) 7309.
[14] Pavarini E., Biermann S., Poteryaev A., Lichtenstein A. I., Georges A. and Andersen O. K., *Phys. Rev. Lett.*, **92** (2004) 176403.
[15] Mochizuki M. and Imada M., *New J. Phys.*, **6** (2004) 154.
[16] Pavarini E., Yamasaki A., Nuss J. and Andersen O. K., *New J. Phys.*, **7** (2005) 188.
[17] Solovyev I. V., *Phys. Rev. B*, **73** (2006) 155117.
[18] Ulrich C., Khaliullin G., Okamoto S., Reehuis M., Ivanov A., He H., Taguchi Y., Tokura Y. and Keimer B., *Phys. Rev. Lett.*, **89** (2002) 167202.
[19] Khaliullin G. and Okamoto S., *Phys. Rev. Lett.*, **89** (2002) 167201.
[20] Kiyama T., Saitoh H., Itoh M., Kodama K., Ichikawa H. and Akimitsu J., *J. Phys. Soc. Jpn.*, **74** (2005) 1123.
[21] Ulrich C., Gössling A., Gruninger M., Guennou M., Roth H., Cwik M., Lorenz T., Khaliullin G. and Keimer B., *Phys. Rev. Lett.*, **97** (2006) 157401.
[22] Li B., Louca D., Hu B., Niedziela J. L., Zhou J. and Goodenough J. B., *J. Phys. Soc. Jpn.*, **83** (2014) 084601.
[23] Kresse G. and Furhmuller J., Software VASP, Vienna (1999); Kresse G. and Hafner J., *Phys. Rev. B*, **47** (1993) R558; **49** (1994) 14251; **54** (1996) 11169; *Comput. Mater. Sci.*, **6** (1996) 15.
[24] Perdew J. P., Burke K. and Ernzerhof M., *Phys. Rev. Lett.*, **77** (1996) 3865; Perdew J. P., Burke K. and Wang Y., *Phys. Rev. B*, **54** (1996) 16533.
[25] Blöchl P. E., *Phys. Rev. B*, **50** (1994) 17953; Kresse G. and Joubert D., *Phys. Rev. B*, **59** (1999) 1758.
[26] Anisimov V. I., Aryasetiawan F. and Lichtenstein A. I., *J. Phys.: Condens. Matter*, **9** (1997) 767.
[27] Maclean D. A., Ng H.-N. and Greedan J. E., *J. Solid State Chem.*, **30** (1979) 35.
[28] Okimoto Y., Katsufuji T., Okada Y., Arima T. and Tokura Y., *Phys. Rev. B*, **51** (1995) 9581.
[29] Kresse G., Furthmüller J. and Hafner J., *Europhys. Lett.*, **32** (1995) 729.
[30] Ye Lin-Hui, Liu Bang-Gui, Wang Ding-Sheng and Han Rushan, *Phys. Rev. B*, **69** (2004) 235409.
[31] King-Smith R. D. and Vanderbilt D., *Phys. Rev. B*, **47** (1992) 1651.
[32] Kovaleva N. N., Boris A. V., Yordanov P., Maljuk A., Brücher E., Strempfer J., Konuma M., Zegkinoglou I., Bernhard C., Stoneham A. M. and Keimer B., *Phys. Rev. B*, **76** (2007) 155125.
[33] Kovaleva N. N., Boris A. V., Capogna L., Gavartin J. L., Popovich P., Yordanov P., Maljuk A., Stoneham A. M. and Keimer B., *Phys. Rev. B*, **79** (2009) 045114.
[34] Stephan W., Capone M., Grilli M. and Castellani C., *Phys. Lett. A*, **227** (1997) 120.
[35] Sangiovanni G., Capone M., Castellani C. and Grilli M., *Phys. Rev. Lett.*, **94** (2005) 026401.
[36] Rošch O. and Gunnarsson O., *Phys. Rev. Lett.*, **93** (2004) 237001.
[37] Sangiovanni G., Gunnarsson O., Koch E., Castellani C. and Capone M., *Phys. Rev. Lett.*, **97** (2006) 046404.
[38] Reznik D., Sangiovanni G., Gunnarsson O. and Devereaux T. P., *Nature*, **455** (2008) E6.